Optimal Sensor Network Design for Multi-Scale, Time-Varying Differential Algebraic Equation Systems: Application to an Entrained-Flow Gasifier Refractory Brick

Qiao Huang and Debangsu Bhattacharyya*

Department of Chemical and Biomedical Engineering, West Virginia University, Morgantown, WV 26506, USA

Abstract

An algorithm for optimal sensor network design for multi-scale, time-varying differential algebraic equation systems with non-separable dynamics is presented. As the process is time-varying, an integral normalized posterior error covariance of a multi-scale filter is minimized to obtain the optimal sensor locations. For reducing the computational cost, an adaptive sampling rate approach is considered for the slowly-varying variables. The algorithm is applied to a smart refractory brick with embedded sensors as part of an entrained-flow gasifier. Thermistors and interdigital capacitors are considered as candidate measurement technologies for estimating temperature and slag penetration profile along the gasifier wall. When the optimal set of sensors obtained from the algorithm is used for estimating temperature and slag penetration profiles in a multi-scale Kalman filter framework, satisfactory estimates are obtained despite high measurement noise and model mismatch.

Keywords

Sensor placement, multi-scale, time-varying, differential algebraic equation, smart refractory, gasifier

---

* Debangsu Bhattacharyya, West Virginia University, Department of Chemical and Biomedical Engineering, Morgantown, WV 26506, USA

Tel:1-304-293-9335, E-mail: Debangsu.Bhattacharyya@mail.wvu.edu

1. **Introduction**

A number of engineered systems evolve over multiple time scales. In various chemical engineering applications, while variables such as species concentration can have time constants of seconds, variables such as the temperature can have time constants of minutes or hours. On the other hand, there are several extremely slow, yet important, mechanisms such as catalyst degradation, heat exchanger fouling that can evolve over weeks or months or even years. Slowly-evolving catalyst degradation in a reactor can affect the temperature dynamics in the reactor while the temperature dynamics in the reactor can affect the dynamics of catalysts degradation. For many such systems, slow and fast dynamics cannot be separated. For control, monitoring, maintenance planning, etc. of such systems, estimation of both slow and fast variables is of utmost importance.

Optimal sensor network design is critical for estimation of the desired variables. The sensor network design problem has been widely studied for single time scale systems. Some measure of estimation error is typically used as the objective of the sensor placement problem (Nabil and Narasimhan, 2012). Estimation accuracy of an optimal filter such as the Kalman filter (KF) is one of the mostly used measures in such sensor network design problems (Sen et al., 2016, 2018). In the work of Musulin et al., time-averaged posterior error covariance matrices calculated over the entire time horizon and asymptotic value of posterior error covariance matrices was used to obtain the optimal sensor network design for a dynamic linear system (Musulin et al., 2005). System observability and sensor network costs were considered as constraints in that work. The sensor network design problem for a nonlinear differential algebraic equation (DAE) system was studied by Mobed et al. (Mobed et al., 2017a, 2017b) using extended KF (EKF).

Typically, process information which can be obtained from a given sensor network increases as the number or the accuracy of the installed sensor increases (Muske and Georgakis, 2003). Therefore, several authors have designed the sensor network taking into account the tradeoff between the process information and the number/cost of sensors. Based on proper orthogonal decomposition and max-min optimization, Alonso et al. proposed a systematic approach to the sensor network design for distributed systems (Alonso et al., 2004). Lee and Diwekar proposed a method to design an optimal sensor network for nonlinear integrated gasification combined cycle power plant by maximizing the overall Fisher information with constraint on the cost of sensors (Lee and Diwekar, 2012). Singh and Hahn proposed a method to determine sensor locations for stable nonlinear dynamic systems with consideration of a tradeoff between process information, information redundancy and sensor cost (Singh and Hahn, 2005, 2006). Jeremy et al. extended the work of Singh and Hahn (Singh and Hahn, 2006) by taking the covariance of empirical observability Gramians into account for the sensor network design (Jeremy et al., 2007). An optimal sensor placement problem has been solved by considering observability and principal component analysis with constraint on number of sensors (Jeremy et al., 2007).

The literature on sensor placement presented before has mainly focused on systems with single time scales or systems where times scales are not significantly different. However there are systems where time scales can be widely different and distinguishing these time scales is desired while designing the sensor network. Furthermore, these systems might exhibit non-separable dynamics and they can be time-varying. To the best of our knowledge, there is no work in the existing literature on the optimal sensor network design for time-varying multi-scale DAE systems with non-separable dynamics. One relevant work in this area is by Kadu et al., who designed the optimal sensor network for time-invariant, multi-rate systems (Kadu et al., 2008). The authors considered different sampling rates for measurements while designing the sensor network. In that work, system estimation accuracy is evaluated by considering a multi-rate KF over a time-horizon. As the traditional KF is applicable to single rate systems, the authors proposed to use updated output (measurement) matrix and measurement error covariance matrix at different sampling instant. Since the dynamics of state estimation accuracy as captured through the Riccati equation are taken into account, the authors considered a large enough time interval for simulation so that the posterior error covariance matrix can reach steady value (Kadu et al., 2008). A straightforward extension of the approach developed by Kadu et al. (2008) to time-varying multi-scale systems has two issues. First, multi-scale time-varying system considered in this paper has at least one order of magnitude difference in the time scales of variables of interest. Since the system error covariance matrix evolves dynamically over a long time, a large enough time interval, such as months or years, is required for the simulation. Second, the multi-scale system can have multiple different sampling rates that can be largely different. As noted out by Kadu et al. (2008) and Gudi et al. (1995), slowly sampled variables can improve observability of the system, reduce variance of the estimates, and reduce sampling requirements of the variables that are sampled faster. However, if the time scale of a variable is very slow, like days, or weeks, then sampling it at a fast rate provides little information. Thus, such multi-scale systems are likely to have very different sampling rates. Due to the issues listed above, a straightforward extension of the approach by Kadu et al. (2008) to time-varying systems with widely varying time scales would lead to an extremely large number of sampling instants that can be computationally intractable. In summary, studies on the sensor network design for time-varying DAE systems with largely different time scales are still limited and highly needed.

The main contribution of this paper is the development of an optimal sensor placement algorithm for time-varying DAE systems with non-separable dynamics and largely different time scales. The optimal sensor network is designed by maximizing the estimation accuracy of the time-varying multi-scale DAE system with constraint on the number of sensors. Due to non-separable dynamics, a bank of filters that are assigned based on the distinct time scales exchanges information while minimizing the error covariance individually. Selection of filtering algorithms depends on a number of criteria including the type of the system (i.e. linear or nonlinear), desired computational expense, user preference, etc. Therefore, one can use different algorithms for different filters in this sensor network design approach. The usefulness of the proposed algorithm is demonstrated by the case of the gasifier smart refractory brick with embedded sensors. Two different kinds of sensors namely, thermistor and interdigital capacitor (IDC) are considered in this study for estimating temperature and slag penetration profiles along the radial direction of gasifier wall respectively.

The rest of this paper is arranged as follows. In Section 2, the optimal sensor placement algorithm is developed. The smart brick system where the algorithm is applied to is presented in Section 3. Results are presented in Section 4 followed by the conclusions.

2. Sensor Placement Algorithm Development

In this section, first, the development of the framework of bank of filters is discussed followed by a discussion on linear and nonlinear filtering algorithms for DAE system. Then, a discussion on adaptive sampling rate used for slowly changing variables is provided, followed by a discussion on the filtering algorithm.

2.1. Multi-scale filter

The multi-scale filtering framework considered in this study is shown in Fig. 1. For simplicity, only two levels are shown in Fig. 1. In Fig. 1, the time scale of the faster variable is designated as the micro scale while that of the slower variable is designated as the macro scale. The figure is developed considering the possibility of an adaptive sampling rate for the macro scale filter. More details on this is provided later. As noted earlier, the time scale separations are done such that minimizing the resulting error covariance calculation individually at each level is equivalent to minimizing the joint error covariance. The error covariance calculation for traditional and extended KFs depends on the state transition matrix, output/measurement matrix, and noise (i.e. measurement and process noise). Therefore, the time scale separation is done such that even if the filters communicate sequentially at the sampling instant of slowest variable, the resulting error in the covariance calculation is low. For more information on the approach similar to this work for simulating a bank of filters, interested readers are referred to the work of Kobayashi and Simon (Kobayashi and Simon, 2003).

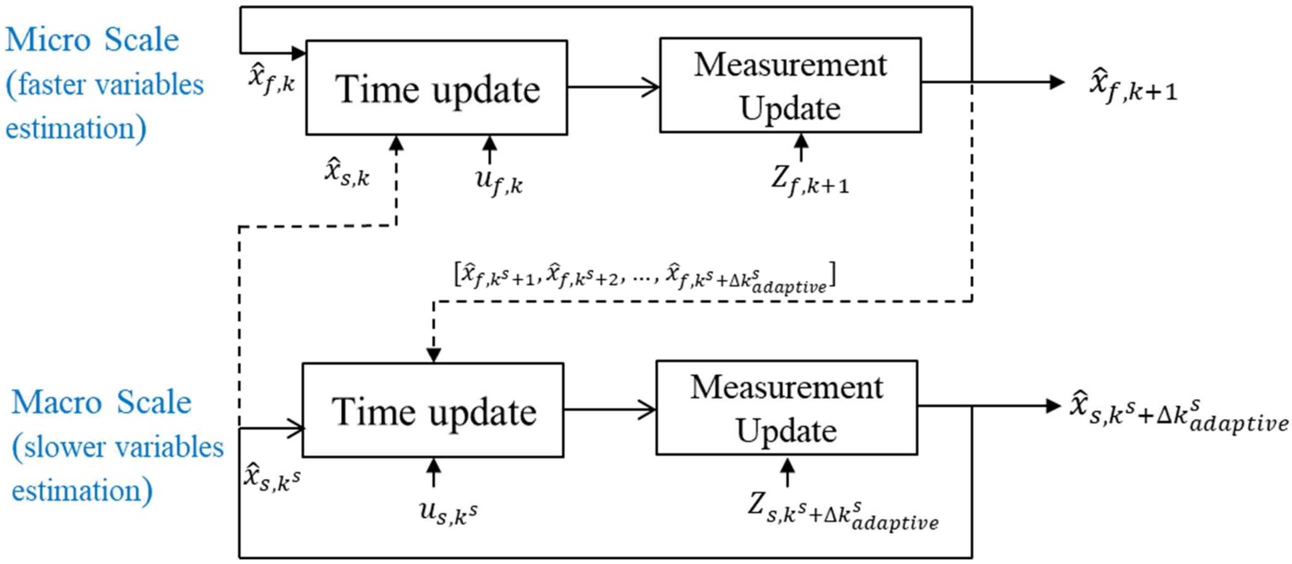

Fig. 1. Schematic description for multi-rate dual KF (dashed lines represent the information exchanges, which happens only when macro scale KF runs)

In this framework, linear or nonlinear filters for ODE/DAE systems can be used at any level. Below, specifically, we firstly describe the filtering approach used for the linear DAE system followed by a discussion on the nonlinear DAE system.

2.2. Modified TKF for the linear DAE system

The linear time-varying DAE system is given by:

$$\dot{x}(t) = D(t)x(t) + G(t)y(t) + M(t)u(t) \quad (1)$$

$$0 = N(t)x(t) + T(t)y(\mathrm{t}) \quad (2)$$

For making the notation compact, in the following, we drop the '(t)' notation from the DAE system given above. Further, differentiating the algebraic equations in Eq. (1),

$$0 = N\dot{x} + T\dot{y} \quad (3)$$

$$\dot{y} = -T^{-1}N\dot{x} = -T^{-1}NDx - T^{-1}NGy - T^{-1}NMu \quad (4)$$

$$\begin{bmatrix} \dot{x} \\ \dot{y} \end{bmatrix} = \begin{bmatrix} D & G \\ -T^{-1}ND & -T^{-1}NG \end{bmatrix} \begin{bmatrix} x \\ y \end{bmatrix} + \begin{bmatrix} M \\ -T^{-1}NM \end{bmatrix} u \quad (5)$$

Eq. (5) can be written as:

$$\dot{x}^{aug} = D^{aug}x^{aug} + M^{aug}u \tag{6}$$

, where $x^{aug} = \begin{bmatrix} x \\ y \end{bmatrix}$, $D^{aug} = \begin{bmatrix} D & G \\ -T^{-1}ND & -T^{-1}NG \end{bmatrix}$, $M^{aug} = \begin{bmatrix} M \\ -T^{-1}NM \end{bmatrix}$

The corresponding discrete-time system along with the measurement equations for the time-varying system can be written as:

$$x_k^{aug} = A_k^{aug}\, x_{k-1}^{aug} + B_k^{aug} u_{k-1} \tag{7}$$

$$z_k = H^{aug}\, x_k^{aug} \tag{8}$$

While the estimation algorithm is similar to the typical TKF algorithm for ODE systems (Maybeck and Siouris, 1980), there are certain differences due to the underlying DAE system. The algorithm is similar to Mandela et al. (Mandela et al, 2010).

Time update:

- A DAE solver is used for calculating a priori state estimate
- A priori covariance matrix is calculated as:

$$\hat{P}_{k|k-1} = A_k^{aug}\hat{P}_{k-1|k-1}A_k^{aug^T} + \gamma_k\hat{Q}_k\gamma_k^T \tag{9}$$

, where $\gamma = \begin{bmatrix} I \\ -T^{-1}N \end{bmatrix}$

Measurement update:

- The Kalman gain and posteriori state estimates are given by:

$$\hat{K}_k = \hat{P}_{k|k-1}H^{aug^T}\left(H^{aug}\hat{P}_{k|k-1}H^{aug^T} + \hat{R}_k\right)^{-1} \tag{10}$$

$$\hat{x}_{k|k}^{aug} = \hat{x}_{k|k-1}^{aug} + \hat{K}_k\left(z_k - H^{aug}\hat{x}_{k|k-1}^{aug}\right) \tag{11}$$

- Using the estimates of the differential states, the posteriori estimates of the algebraic states are obtained by solving the algebraic equations. i.e. Eq. (2).
- The posteriori estimate of the covariance matrix is given by:

$$\hat{P}_{k|k} = (I - \hat{K}_k H^{aug})\hat{P}_{k|k-1} \quad (12)$$

2.3. Nonlinear filter

For nonlinear filtering, the EKF is considered here even though other nonlinear filters can be used. Given the following nonlinear process,

$$\dot{x}(t) = f(x, y, u, w, t) \quad (13)$$

$$0 = g(x, y, t) \quad (14)$$

$$z = h(x, y, v, t) \quad (15)$$

with $w \sim (0, Q)$, $v \sim (0, R)$

For estimating the error covariance in EKF, a linearized system similar to Eqs. (1)-(2) is generated where:

$$D = \frac{\partial f}{\partial x}, G = \frac{\partial f}{\partial y}, M = \frac{\partial f}{\partial u}, N = \frac{\partial g}{\partial x}, T = \frac{\partial g}{\partial y}$$

Then the similar approach as in Section 2.2 is used except the following differences - at the time update step, the DAE solver is used considering Eqs. (13)-(14) for calculating the a priori state estimates; at the measurement update step, once the posteriori estimates of the differential states are obtained, the algebraic states are calculated by using Eq. (14), and Eq. (11) is modified as:

$$\hat{x}^{aug}_{k|k} = \hat{x}^{aug}_{k|k-1} + \hat{K}_k \left(z_k - h\left(\hat{x}^{aug}_{k|k-1} \right) \right) \quad (16)$$

In addition, $H^{aug} = \begin{bmatrix} \frac{\partial h}{\partial x} & \frac{\partial h}{\partial y} \end{bmatrix}$

Other details of standard EKF algorithm can be found in the literature (Haykin, 2001).

2.4. Adaptive sampling rate for the slowly changing variable

Since the computational burden for the filter corresponding to the slowly changing variable can be high due to the long time window that may be needed, an adaptive sampling rate can be considered by exploiting the possibility that the rate of change of the error covariance matrix can considerably change in course of time. The approach for calculating the adaptive sampling rate is similar to the work of Jain and Chang (2004).

Suppose the difference between model results using adaptive and uniform (fast) sampling rate is given by:

$$\delta_k = |\theta_k - \bar{\theta}_k| \quad (17)$$

where θ_k and $\bar{\theta}_k$ represent model results using adaptive and uniform sampling rates respectively.

The weighted average difference is calculated by considering the *j* most recent difference terms:

$$\Delta_k = \frac{\sum_{j=1}^{J} \delta_{k-j+1}/j}{\sum_{j=1}^{J} 1/j} \quad (18)$$

The sampling interval for the next iteration is calculated by:

$$\tau_{k+1} = \tau_k + \gamma\left(1 - e^{\frac{\Delta_k - \lambda}{\lambda}}\right) \quad (19)$$

where τ_{k+1} is sampling interval for k+1 time step; λ is target error; and γ is the parameter that controls the rate of the sampling interval changes.

2.5. Sensor placement algorithm

The objective function for the sensor placement algorithm is considered to be the integral weighted posterior error covariance matrix from the multi-scale KF as follows:

$$\min \left[\sum_{i=1}^{n} w_i F_{i,c}^{N}\right]$$

$$\text{s.t.} \quad (20)$$

$$\sum_{j=1}^{m} C_j S_j \leq C^{max}$$

$$S_j \in S^{+}, j = 1 \ldots m$$

where w is a weighting vector, S_j is a non-negative integer decision variable. S^{+}denotes the candidate set. C_j denotes some factor such as cost associated with the sensor *j*. If it is desired to constrain the maximum number of sensors instead of cost, then $C_j = 1$. $F_{i,c}^{N}$ is normalized fitness value for x^i. The case where all states are measured is considered to be the “best” case, while the case where no sensor is placed is considered to be the “worst” case. Let $k_i = 1 \ldots T_i$ be the time horizon for simulation. The normalized posterior error covariance corresponding to variable *i* over the entire time horizon can be calculated with respect to the “best” and “worst” cases as follows:

$$F_{i,c}^{N} = \frac{F_{i,c} - F_{i,b}}{F_{i,w} - F_{i,b}} \quad (21)$$

, where $F_{i,c} = \frac{1}{T_i}(\sum_{k_i=1}^{T_i} \text{trace}\,(\hat{P}_{k_i}))$

This optimal sensor placement problem can be solved by many integer programming algorithms, such as genetic algorithm (GA) (Paul et al., 2015, 2016), tree search algorithm (Nguyen and Bagajewicz, 2008, 2012), etc. For the specific case when it is solved by GA, Fig. 2 shows the algorithm for solving this multi-scale optimal sensor placement problem.

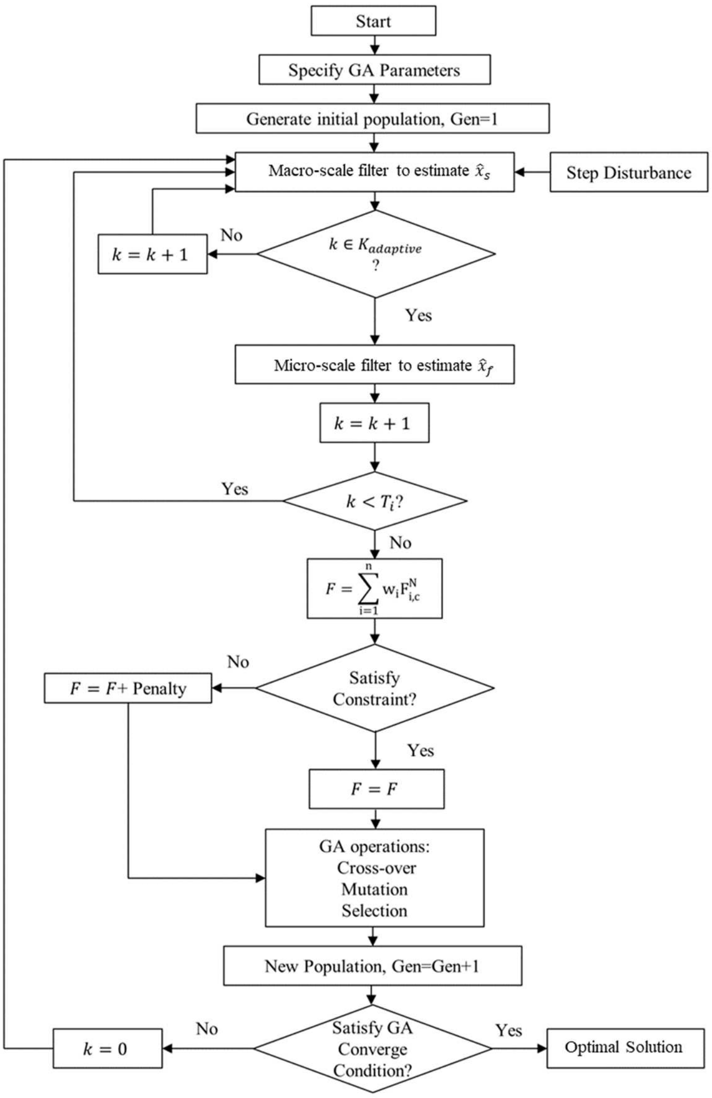

Fig. 2. Optimal sensor placement algorithm for multi-scale system ($K_{adaptive}$ represents adaptive sampling time series, T_i represents the maximum time step for simulation)

3. Case Study: Smart Refractory Brick for Gasifiers

The proposed sensor placement algorithm is applied to a smart brick system as part of an entrained-flow gasifier. Gasifiers are at the heart of the integrated gasification combined cycle plants (Jiang and Bhattacharyya, 2014). Temperature (Seenumani et al., 2012) and extent of slag penetration (Ramalakshmi et al., 2014) are the two most important variables for structural health monitoring (SHM) of slagging gasifiers (Pednekar et al., 2016a, 2016b). In our previous work, we have communicated the possibility of constructing the gasifier wall using a 'smart' refractory brick, a brick with embedded sensors, for estimating the temperature profile in the gasifier wall and extent of slag penetration in the refractory (Huang et al., 2017a, 2017b).

Optimal sensor network design can be helpful for monitoring the long-term structural degradation (Ansari, 2005). However, in a smart brick, there are large numbers of candidate locations for placing sensors. Depending on the type of sensor placed in a given location, it may be possible to obtain information on multiple variables of interest (Paul et al., 2017). In practical SHM systems, it is not feasible to measure all variables of interest at all candidate locations (D'souza and Epureanu, 2008). Sensors can only be placed in a limited number of locations due to budget constraint, structural inaccessibility and so on (Sun and Büyüköztürk, 2015). Large number of sensors embedded in the smart brick can also compromise the structural integrity of the brick. Furthermore, sensors may be redundant, i.e. the measurements provide no or negligible additional information. While redundant measurements may be helpful for increasing the reliability of the sensor network, such redundant measurements need to be optimally selected with due consideration of the sensor failure probability. The gasifier system is multi-scale in nature. While the time constant of temperature is in the order of minutes, that of slag penetration is in hundreds of hours (Huang et al., 2017b). For this system, dynamics cannot be separated. The molten slag that penetrates into the refractory lining leads to changes in the refractory thermal properties (i.e. heat capacity and thermal conductivity). Therefore, the temperature profile in gasifier wall will be affected not only by the temperature on the hot face, but also by the extent of slag penetration. On the other hand, a change in the temperature profile leads to a change in the slag viscosity. As a result, the extent of slag penetration will be affected by temperature, too. It is desired to design the optimal sensor network for this time-varying, multi-scale system with inseparable dynamics. Two different kinds of sensors namely, thermistor and IDC are considered in this study to detect temperature and extent of slag penetration respectively. Unlike the most types of sensors used in SHM, IDC can only be sensitive to slag within a limited distance (Gevorgian et al., 1996) and the length of this sensitive distance depends on the installation direction of IDC. Therefore, the installation direction of the IDC is determined in this work through sensitivity analysis. After that, the optimal sensor network in the smart refractory brick is designed by using the proposed algorithm. The resulting optimization problem is solved by GA.

3.1. Process models

Smart brick is a brick with sensors embedded in it. As discussed in our previous publication (Huang et al., 2017b), these bricks are intended to be placed in the high chromia layer of gasifier wall to detect wall temperature profile and extent of slag penetration. The layout of gasifier's refractory wall with smart brick is shown in Fig. 3. The goal of this paper is to determine the optimal sensor locations for this smart brick. The model of the gasifier where the refractory is considered can be found in our previous publications (Kasule et al. 2014, 2012).

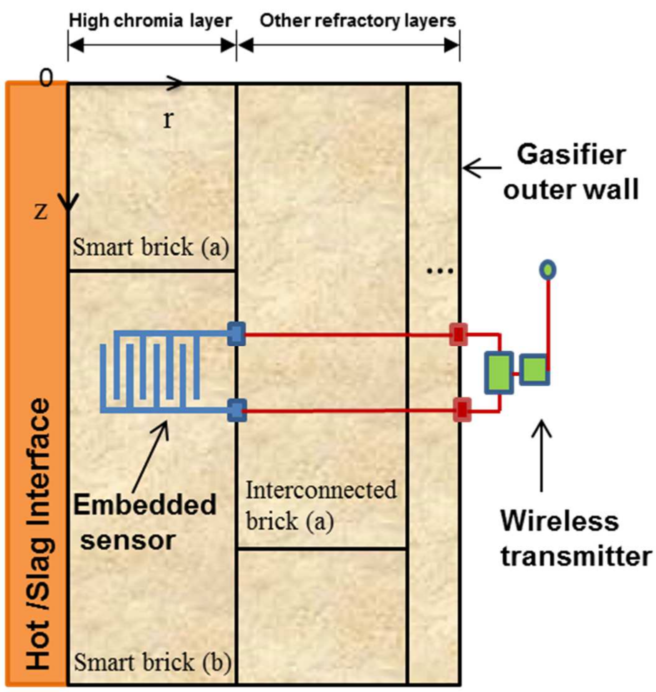

Fig. 3. Schematics of the refractory wall with smart refractory brick

The thermal model for a given refractory brick is developed considering conduction to be the dominant heat transfer mechanism through the wall. At all boundaries between the layers, temperature and flux continuities are assumed. The 2-D governing equation for the thermal model is as follows:

$$\frac{\partial(\rho C_p \hat{T})}{\partial t} = \left(\frac{1}{r}\frac{\partial}{\partial r}\left(rK\frac{\partial \hat{T}}{\partial r}\right) + \frac{\partial}{\partial z}\left(K\frac{\partial \hat{T}}{\partial z}\right)\right) \tag{26}$$

In Eq. (26), material properties such as ρ, C_p, K are time-varying. The refractory properties depend on both the change in the temperature and extent of slag penetration. The effective properties of slag-infiltrated brick are calculated using mixing rules by using its composition. For more details about the thermal and property models, readers are referred to our previous publications (Huang et al., 2017a, 2017b).

The modified Washburn equation (Washburn, 1921) with correction for the tortuosity of the refractory pore system is used to evaluate the slag penetration depth. Sag penetration is modeled by (Carbonell et al., 2004):

$$\frac{dl}{dt} = \frac{\Delta P R^2}{8\eta\sigma^2 l} \tag{27}$$

where ΔP is the pressure drop across refractory lines, R is the refractory pore radius, η is slag viscosity, σ is the tortuosity, and l is infiltration length. More details of models and model parameter values can be found in our previous publications (Huang et al., 2017a, 2017b).

3.2. Sensor models

Two kinds of sensors, namely thermistor and IDC, are considered in this optimal sensor network design problem. The layouts of the thermistor and IDC are shown in Fig. 4.

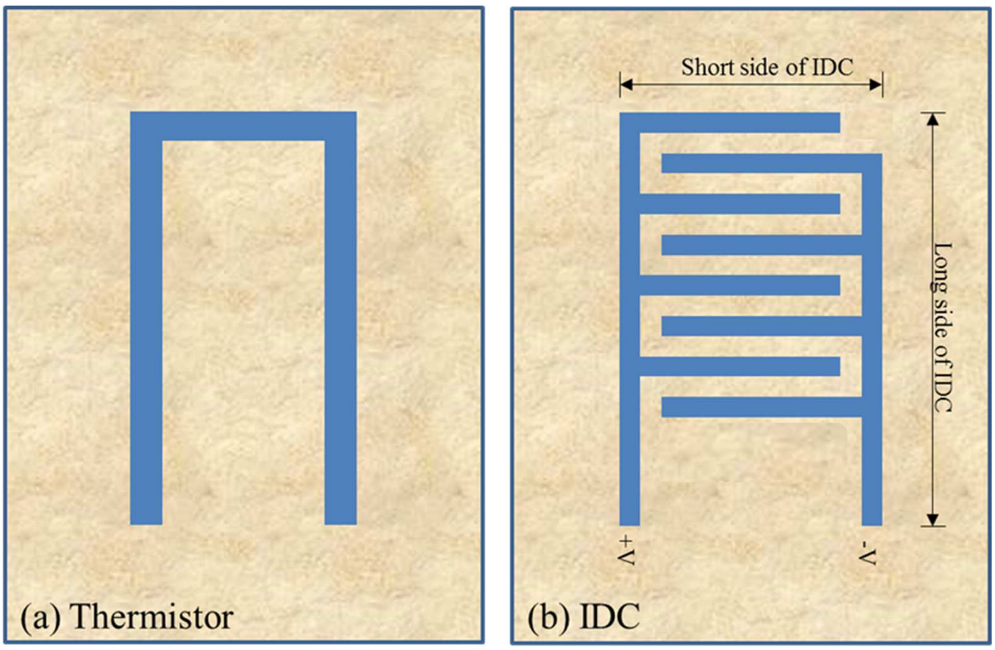

Fig. 4. Schematics of the smart brick with layouts of the (a) the thermistor, and (b) IDC

Thermistor is sensitive to temperature mainly because the electrical conductivity of the sensor is more than 200 times higher than the slag (Huang et al., 2017b) and, therefore, the extent of slag penetration is unlikely to affect the thermistor response. The equivalent circuit method is employed to model the thermistor as given below, where the overall resistance of a given thermistor is calculated by summing the resistance of the sensor material in each control volume where it exists:

$$R = \sum_{i=1}^{n} \frac{\zeta_i \Delta L_i}{\alpha_i} \quad (28)$$

It should be noted that there is considerable spatial variation in the temperature not only along the width of the smart brick, but even along the length of the thermistor. Therefore, spatially distributed and temperature-dependent electrical conductivity, ζ, for the WSi_2-Al_2O_3 thermistor is considered in this work. More details about the thermistor model can be found in our previous work (Huang et al., 2017b).

The IDC model is developed using a conformal mapping technique where the sensor is mapped to an equivalent parallel plate capacitor for easy computation of its response (Igreja and Dias, 2004). Both the extent of slag penetration and temperature affect the refractory dielectric constant considerably and, therefore, affecting the resistance of the IDC sensor. The model also considers the temperature-dependent dielectric constant of the high-chromia refractory, which is the host refractory material (Huang et al., 2017b).

In this model, the n^{th} electrode's interior half-capacitance of a layer m under the electrode plane, $C_{Iu,m}^{n}$, and the n^{th} electrode's exterior half-capacitance of a layer m under the electrode plane, $C_{Eu,m}^{n}$, are given by the equations below:

$$C_{Iu,m}^{n} = \varepsilon_0 L(\varepsilon_{m,u}^{n} - \varepsilon_{m+1,u}^{n}) \frac{K_e(k_{m,I})}{K_e(k'_{m,I})} \quad (29)$$

$$C_{Eu,m}^{n} = \varepsilon_0 L(\varepsilon_{m,u}^{n} - \varepsilon_{m+1,u}^{n}) \frac{K_e(k_{m,E})}{K_e(k'_{m,E})} \quad (30)$$

where ε_0 and ε are vacuum permittivity and relative dielectric constant, respectively, and L is the length of the IDC finger. It should be noted that the equations above are highly nonlinear partly because of $K_e(.)$, that denotes the complete elliptic integral of first kind with modulus $k_{m,I}, k_{m.E}$ and complementary modulus $k'_{m,I}$ and $k'_{m,E}$ corresponding to the interior and exterior electrode planes, respectively. Furthermore, these moduli are dependent on the electrode design parameters such as the width of the IDC fingers, distance between the IDC fingers, and the thickness of the dielectric layer. Similarly, the electrode's interior half-capacitances of layers above the electrode plane, $C^n_{Ia,m}$, and the electrode's exterior half-capacitances of layers above the electrode plane, $C^n_{Ea,m}$, are obtained.

The n[th] electrode total exterior capacitance, C^n_E, is calculated by using the partial capacitance technique where the exterior layer capacitances above and under the sensor plane are summed.

$$C^n_{E,a} = C_{E,a\infty} + \sum_{m=1}^{Ns} C^n_{Ea,m} \tag{31}$$

$$C^n_{E,u} = C_{E,u\infty} + \sum_{m=1}^{Ns} C^n_{Eu,m} \tag{32}$$

$$C^n_E = C^n_{E,a} + C^n_{E,u} \tag{33}$$

It should be noted that N_s, the number of sensitive layers, in the equations above depend on a specific system. More discussion on this is provided in the next section. Similarly, the total interior electrode capacitance, C^n_I, can be calculated. Then the total capacitance of IDC sensor can be calculated by C^n_I and C^n_E using equivalent circuit analysis. Interested readers are referred to our previous publication for more details of the IDC model (Huang et al., 2017b). The IDC sensor model is highly nonlinear and therefore, linearization of this model, if used in a linear estimator, can lead to high inaccuracies.

3.3. IDC sensitive distance analysis

Since thermistor is not directly sensitive to the extent of slag penetration, IDC is the only type of sensors used to measure the extent of slag penetration. However, it was observed in our previous study that the embedded IDC sensors are only sensitive to the slag penetration in a short distance (Huang et al., 2017b). Once the slag penetrates beyond this sensitive area, IDC measurements are not expected to change due to further slag penetration. Therefore, unlike the thermistor for which the installation direction is not expected to play a big role in temperature profile estimation, the installation direction of the IDCs does have a strong impact and, therefore, should be carefully selected. Fig. 5 shows two installation directions which are evaluated in this work.

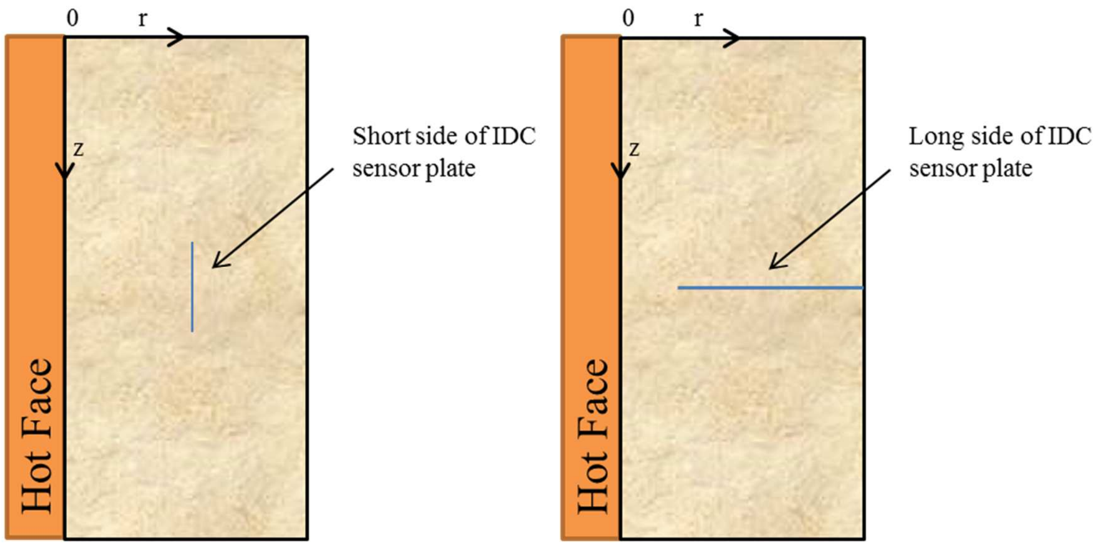

(a) IDC is installed parallel to hot face (b) IDC is installed perpendicular to hot face

Fig. 5. Installation directions of IDC considered in the study

3.4. Implementation of the sensor placement algorithm.

In this work, it is assumed that the modified TKF is used for estimating temperature (i.e. fast-changing variable) while for estimating slag penetration depth (i.e. slowly changing variable), the EKF is used due to the high nonlinearity of the penetration model and the sensor model. Since the slag penetration rate varies significantly with time, adaptive sampling rate is employed for slag penetration depth estimation. Due to the change in the material properties as a result of continuing slag penetration, the process becomes time-varying. Therefore, the corresponding process covariance matrix evolves until slag penetrates through the high-chromia layer. Since the embedded sensors in the refractory are novel and the manufacturing process is still being improved, no cost data for the sensors are currently available. Therefore, instead of a constraint on the maximum cost in the sensor placement problem, it was decided to consider a constraint on the maximum number of sensors. The sensor placement problem is solved using the GA algorithm with parallel computing toolbox in MATLAB 2016a. The population size and maximum generation number of GA are chosen to be 50 and 30, respectively.

4. Results and discussion

4.1. Impact of installation direction on the sensitivity of IDC to slag penetration depth

The capacitance of the IDC can change as a result of change in the dielectric constant due to change in the temperature, slag penetration depth, or both. In this study, the temperature is set to be constant at 1400°C.

The IDC is assumed to be placed on the center of ‘smart’ refractory. The IDC geometry parameters *W, G, L* as shown in Fig. 4(b) are set to be 0.5 cm, 0.5 cm and 0.3758 cm, respectively. Total number of fingers is specified to be 8 in this section. Fig. 6 shows how the capacitance changes as slag penetrates into the smart refractory brick when IDC installed as shown in Fig. 5 (a), i.e. when the IDC is placed parallel to the hot face.

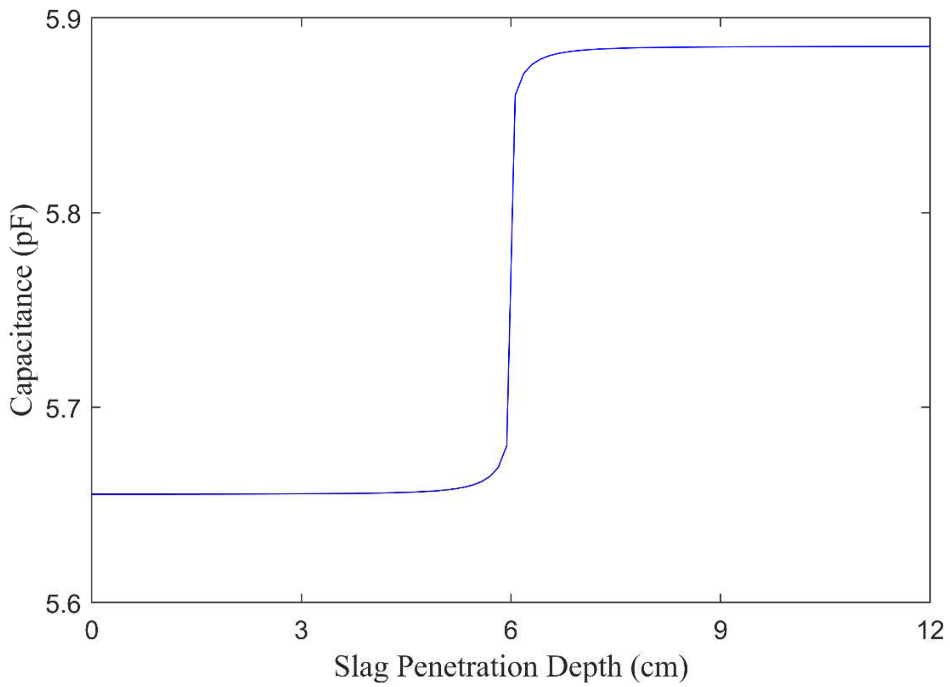

Fig. 6. Sensitivity of IDC to slag penetration depth when the sensor is placed parallel to the hot face

As observed in Fig. 6, the capacitance of IDC increases sharply when slag passes through the sensor plane, but before and after that, it remains largely insensitive in the radial direction, which is of main interest. Thus, this orientation will lead to a large number of IDCs. It should be noted that the sensitive distance of IDC in the direction perpendicular to the sensor plate can change as the sensor dimension changes. (Igreja and Dias, 2004) However, the impact of this change is very limited. Another option is to place the sensor perpendicular to the gasifier hot face. Fig. 7 shows the change in the capacitance due to slag penetration when IDC installed as shown in Fig. 5 (b), i.e. perpendicular to the hot face.

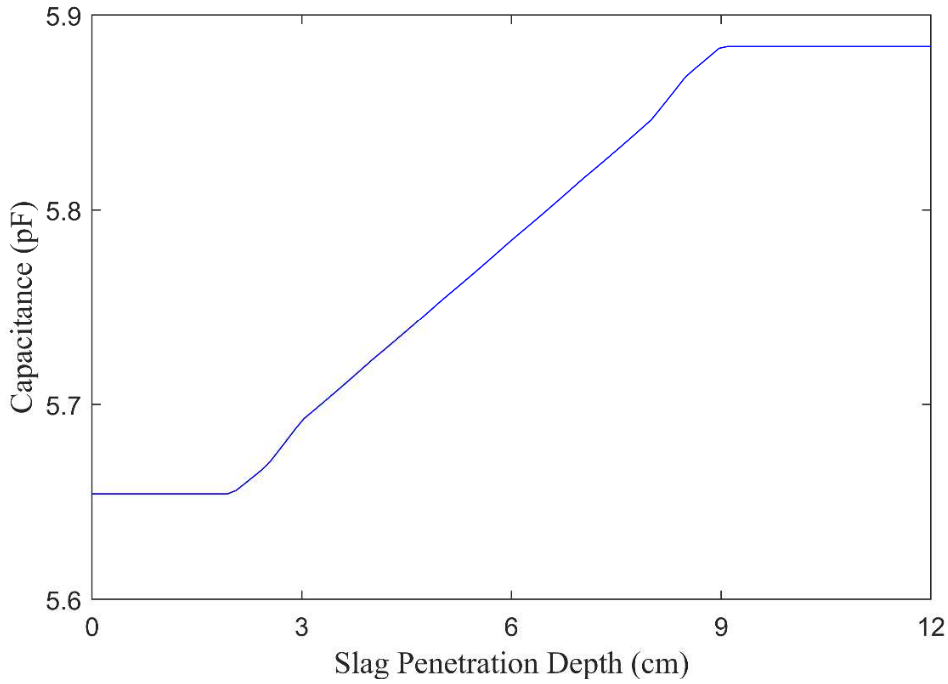

Fig. 7. Sensitivity of IDC to slag penetration depth when the sensor is placed perpendicular to the hot face

As shown in Fig. 7, the sensitive distance for this IDC is 7 cm, which is the length of this IDC sensor. In this work, extent of slag penetration is of interest only in the high-chromia layer. If the length of IDC is designed to be the thickness of high-chromia layer, then the extent of slag penetration through the entire high-chromia layer can be estimated. Therefore, this long IDC placed perpendicular to the hot face is considered to be used in the 'smart' refractory brick for estimating slag penetration depth. Therefore, optimal placement of only the thermistors need to be considered.

4.2. Optimal thermistor placement based on multi-scale KF

Fig. 8 shows the candidate sensor locations in smart refractory brick. The long IDC is placed on the centerline of this smart brick. The algorithm developed in Section 2 is applied to obtain the optimal thermistor placement. The reason of using two KFs in this case study, even though only the placement of thermistors needs to be optimally selected, is that the covariance estimates of both filters are affected due to the placement of thermistors. This can be understood by analyzing the time-varying process. The slag penetration rate strongly depends on the temperature. If the temperature is low, the slag penetration rate can considerably drop due to the significant change in the slag viscosity as seen in Eq. (27). On the other hand, slag infiltration affects the material properties such as the specific heat and thermal conductivity thereby affecting its temperature profile for given boundary conditions. Since the slag infiltrates through the high temperature region reasonably quickly, a large number of thermistors in these regions is not helpful for improving the estimation accuracy, rather the thermistors placed in relatively lower temperature regions provide valuable information for long period of time as the slag infiltrates through these regions relatively slower and, therefore, improves the integral covariance estimates. These aspects can be observed in the results presented below.

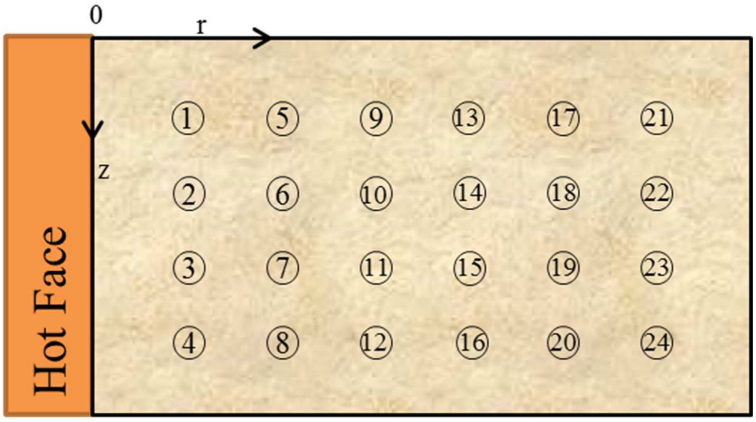

Fig. 8. Candidate sensor locations for thermistors in the 'smart' refractory brick

Weighting factors, w_i, in the objective function for sensor placement (Eq. (20)) are set to be 1. The time interval of the simulation is chosen to be long enough so that the slag penetrates through the entire smart brick (high-chromia layer). This is done so that the effect of this time-varying process can be captured while designing the sensor network. Table 1 shows the optimal results when the maximum number of sensors are set to be 8 and 16 thermistors.

Table 1. Optimal placement for 8 and 16 thermistors

Number of Sensor Installed	Optimal Locations
8	8, 10, 13, 16, 20, 21, 22, 24
16	6, 8, 9, 10, 11, 12, 13, 14, 16, 17,19, 20, 21, 22, 23, 24

It can be observed in Table 1 that the constraint on maximum number of sensors are reached for both cases. It is also observed that more number of thermistors are placed near the colder side of the smart refractory. As discussed before, thermistors placed near the colder side improves the covariance estimate for long time duration. Obviously this aspect is exploited by the optimizer for minimizing the integral error covariance of this time-varying process.

Fig. 9 shows how the normalized fitness value for the temperature and slag penetration depth change with respect to the number of thermistors.

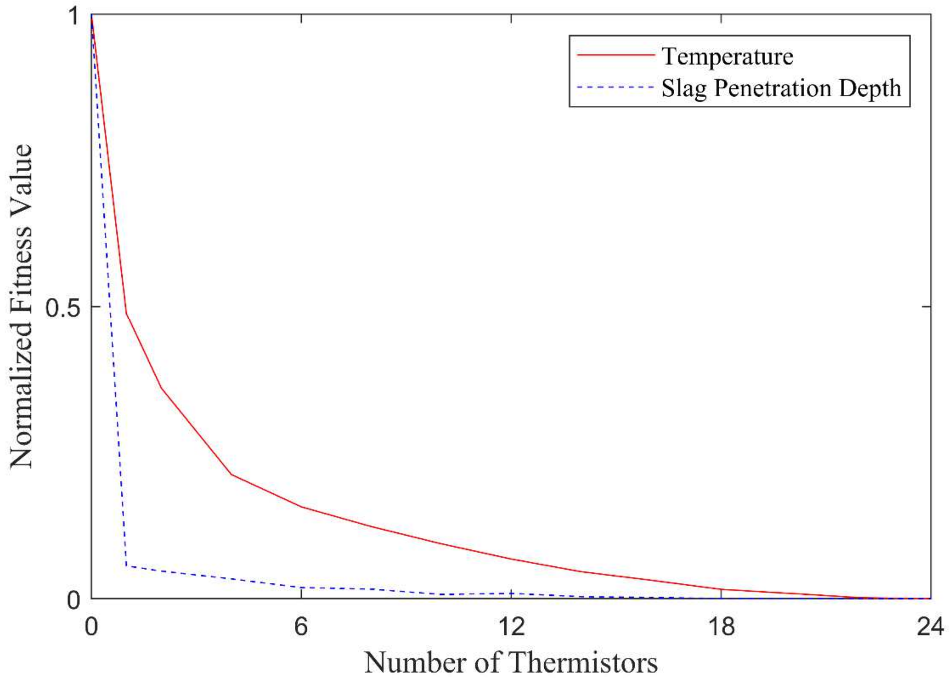

Fig. 9. Sensitivity of normalized fitness value for slag penetration depth and temperature to the number of thermistors

It can be observed that the estimation error in slag penetration depth decreases quickly as the number of thermistor increases from 0 to 1. It is because the accuracy of temperature estimates has a strong effect on the estimation accuracy of slag, but a highly accurate estimation of temperature is not required for improving the estimation accuracy of slag penetration depth. These results also show why both the filters need to be considered together even though only placement of thermistors is being considered by the sensor placement algorithm.

4.3. Estimation of slag penetration depth and temperature with optimal sensor network

As discussed in the previous section, estimation accuracy does not improve much beyond 8 thermistors. Therefore, 8 thermistors with a long IDC placed in the centerline is considered to be the optimal sensor network for this smart refractory brick. The system considered here is a complex system with expected mismatches between the actual system and the model. Therefore, it is desired to study the estimator performance at the face of model mismatch. Model mismatch is simulated by using different sets of parameters between the 'true' process and the KF model for calculation of the specific heat of the slag-infiltrated refractory brick and the slag viscosity. The performance of this sensor network is studied using the multi-scale KF by simulating a 50°C step increase in the hot face temperature introduced at t=0. Estimation of resistance and temperature at sensor location #8 is shown in Figs. 10(a) and 10(b), respectively.

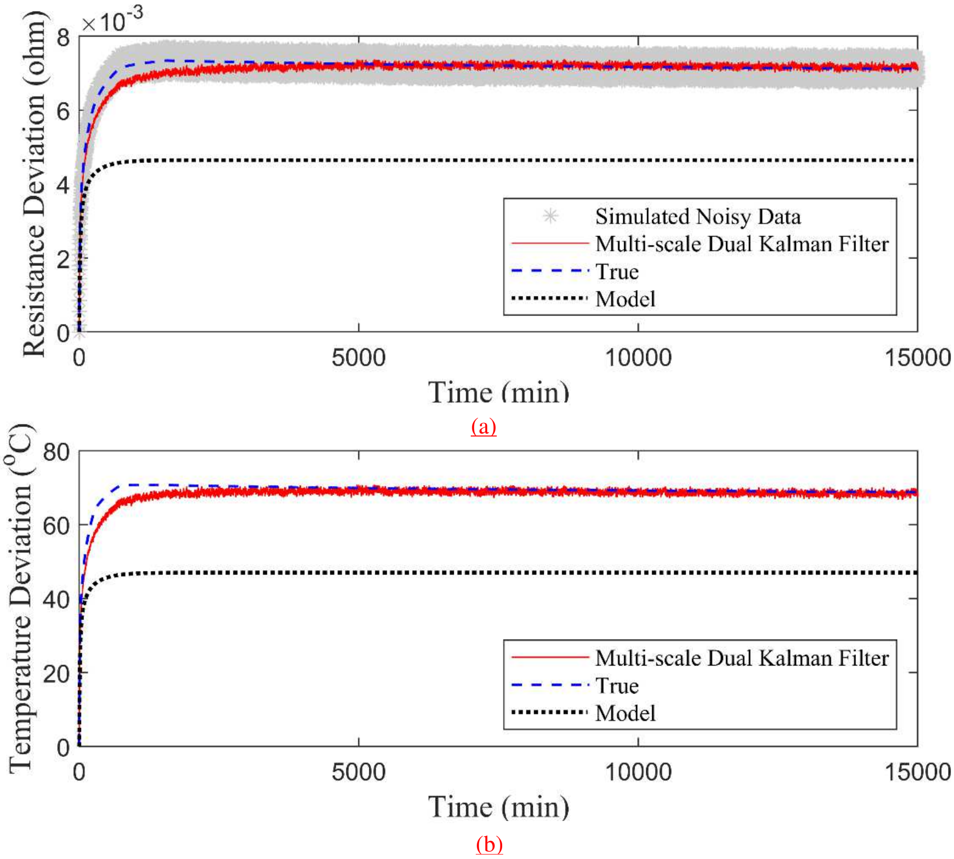

Fig. 10. Estimates using the multi-scale KF and measurements from the optimal sensor network for: (a) resistance, (b) temperature

As it shown in Fig.10(b), temperature at sensor location #8 increases by about 66°C due to the 50°C step increase in the hot face. It is because a higher temperature increases slag penetration depth and a brick with higher extent of slag penetration has higher thermal conductivity, thus increasing its temperature more than the increase in the boundary temperature. More details about how slag penetration affects temperature profile of gasifier's refractory wall can be found in our previous work (Huang et al., 2017b).

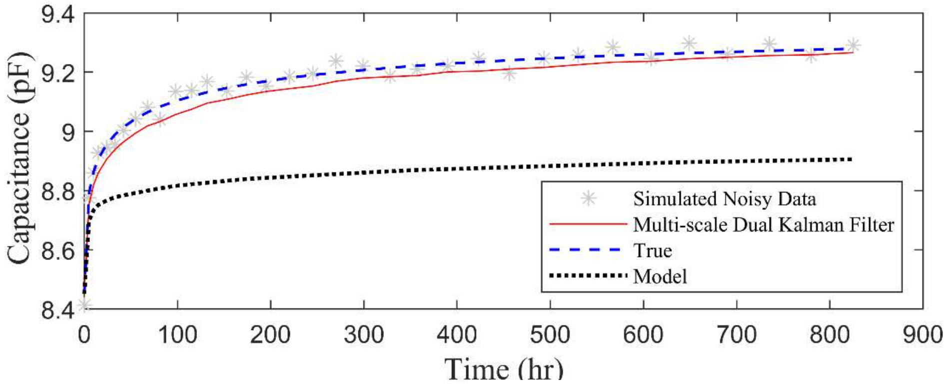

(a)

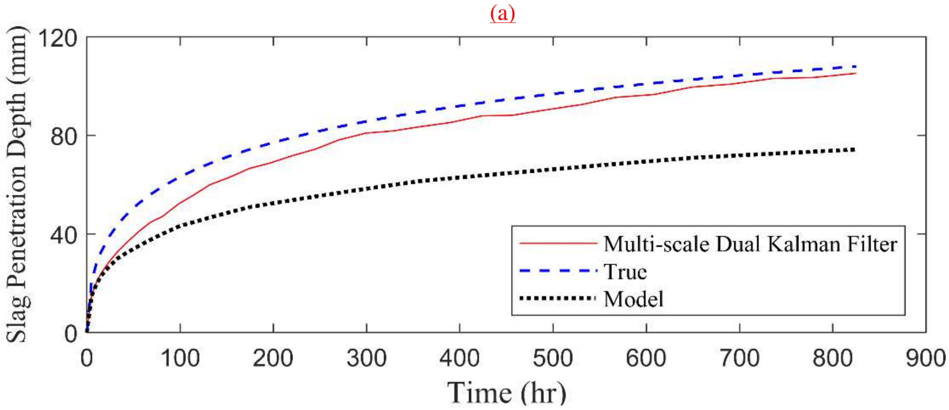

(b)

Fig. 11. Estimates using the multi-scale KF and measurements from the optimal sensor network for: (a) capacitance, (b) slag penetration depth

Fig. 11 shows the estimates of slag penetration depth and capacitance using the multi-scale KF. As observed in Fig. 11(b), even though the measurements are noisy and there is large discrepancy in the model, the optimal sensor network results in a highly accurate estimate of the slag penetration depth.

5. Conclusion

In this paper, an algorithm to design an optimal sensor network for multi-scale, time-varying DAE systems has been developed. The integral normalized posterior error covariance of the multi-scale KF is minimized to obtain the optimal sensor locations. In order to reduce the computational cost, the adaptive sampling rate has been used for the slowly-varying variables. Sensor placement problem for a smart refractory brick has been used as a case study to illustrate the presented algorithm. For this case, the sensitivity of IDC installation direction to slag penetration depth has been analyzed first. IDC placed perpendicular to the hot face is found to be more sensitive to slag penetration depth and is used in the following case study. Then, the optimal thermistor locations have been obtained by using the proposed algorithm. The GA is used to solve the optimization problem. Finally, using the multi-scale KF framework (i.e. two KFs for two different time scales) with the thermistor and IDC sensors embedded in the given optimal locations, it is found to provide satisfactory estimates for both the temperature profile and extent of slag penetration despite high measurement noise and model mismatch. Even though a system with two time-scales is considered as the case study in this paper, the proposed algorithm can be easily applied to systems with multiple time scales by using a bank of filters. In addition, even though the TKF and EKF are used in this case study, other linear/nonlinear estimators can also be considered in the proposed framework.

Acknowledgements

Authors gratefully acknowledge financial support for this research by DOE [grant number DE-FE0012383] titled "Smart Refractory Sensor Systems for Wireless Monitoring of Temperature, Health, and Degradation of Slagging Gasifiers".

Nomenclature

C_p	heat capacity ($J/g \cdot$°C)
K	thermal conductivity ($W/m \cdot$°C)
$\hat{T}$	temperature (°C)
R	pore radius (m)
l	infiltration depth (mm)
ΔL	Length of the thermistor in a given control volume
ΔP	pressure difference across refractory lines
W	width of the IDC finger (cm)
G	distance between the IDC fingers (cm)
L	length of IDC finger (cm)
k	time step, modulus
k'	Complementary modulus
$\Delta k_{adptive}$	adaptive time step
$\hat{T}_s$	estimated temperature from micro-scale KF (°C)
$\hat{l}$	estimated infiltration depth from macro-scale EKF(mm)
x	vector of differential variables
y	vector of algebraic variables
u	vector of system inputs
z	measurements
$\hat{Q}$	process noise covariance matrix
$\hat{R}$	measurement noise covariance matrix
$\hat{K}$	augmented Kalman gain
w	Weighting factor, process noise

S	non-negative integer decision variable
S^+	the candidate set
C	factor
C^{max}	constant
N	designed number of sensors
T	simulation time

Greek letters

ρ	density (kg/m^3)
ε_0	vacuum permittivity (F/m)
ε	relative dielectric constant
α	cross-sectional area of the thermistor (m^2)
η	slag viscosity ($Pa.s$)
σ	tortuosity of refractory pore system
θ	model prediction using adaptive sampling rate
$\bar{\theta}$	model prediction using fast uniform sampling rate
δ	difference between model predictions using adaptive and fast uniform sampling rates
τ	sampling interval
λ	target error
ζ	Electrical resistivity of sensor
γ	parameter that controls the rate of sampling interval changes

Subscripts

j	j^{th} candidate sensor
IDC	interdigital capacitor
k	time step k
i	i^{th} state variable/control volume
m	m^{th} layer
c	current
w	worst
b	best

Superscripts

aug	augmented
N	normalized
n	n^{th} electrode of IDC

Acronyms

IDC	interdigital capacitor
KF	Kalman filter

EKF	extended Kalman filter
DAE	differential algebraic equations

References

Ansari, F., 2005. Sensing Issues in Civil Structural Health Monitoring. Springer, Dordrecht.

Alonso, A.A., Kevrekidis, I.G., Banga, J.R. Frouzakis, C.E., 2004. Optimal sensor location and reduced order observer design for distributed process systems. Comput. Chem. Eng. 28, 27-35. https://doi.org/10.1016/S0098-1354(03)00175-3

Carbonell, S., Hey, M.J., Mitchell, J.R., Roberts, C.J., Hipkiss, J., Vercauteren, J., 2004. Capillary flow and rheology measurements on chocolate crumb/ sunflower oil mixtures. J. Food Sci. 69, 465-470. https://doi.org/10.1111/j.1365-2621.2004.tb09931.x

D'souza, K., Epureanu, B.I., 2008. Sensor placement for damage detection in nonlinear systems using system augmentations. AIAA J. 46, 2434-2442. https://doi.org/10.2514/1.33493

Gevorgian, S.S., Martinsson, T., Linner, P.L., Kollberg, E.L., 1996. CAD models for multilayered substrate interdigital capacitors. IEEE Trans. Microw. Theory Tech. 44, 896-904. https://doi.org/10.1109/22.506449

Gudi, R.D., Shah, S.L., Gray, M. R., 1995. Adaptive multirate state and parameter estimation strategies with application to a bioreactor. AIChE J. 41, 2451-2464. https://doi.org/10.1002/aic.690411111

Haykin, S.S., 2001. Kalman Filtering and Neural Networks. Wiley, New York.

Huang, Q., Bhattacharyya, D., Pillai, R., Sabolsky, K., Sabolsky, E.M., 2017a. Gasifier health monitoring using smart refractory bricks. Proceedings of 11th International Workshop on Structural Health Monitoring, Stanford University, CA, September 12-14, 2017. https://doi.org/10.12783/shm2017/14160

Huang, Q., Paul, P., Bhattacharyya, D., Pillai, R. C., Sabolsky, K., Sabolsky, E.M., 2017b. Estimation of gasifier wall temperature and extent of slag penetration using a refractory brick with embedded sensors. Ind. Eng. Chem. Res. 56, 9858-9867. https://doi.org/10.1021/acs.iecr.7b02604

Igreja, R., Dias, C.J., 2004. Analytical evaluation of the interdigital electrodes capacitance for a multi-layered structure. Sens. Actuators A Phys. 112, 291-301. https://doi.org/10.1016/j.sna.2004.01.040

Jain, A., Chang, E.Y., 2004. Adaptive sampling for sensor networks. Proceedings of the 1st International Workshop on Data Management for Sensor Networks: in Conjunction with VLDB 2004. Toronto. https://doi.org/10.1145/1052199.1052202

Jeremy, B., Huang, Z., Singh, A.K., Misra, M., Hahn, J., 2007. Sensor network design via observability analysis and principle component analysis. Ind. Eng. Chem. Res. 46, 8026-8032. https://doi.org/10.1021/ie070547n

Jiang, Y., Bhattacharyya, D., 2014. Plant-wide modeling of an indirect coal-biomass to liquids (CBTL) plant with CO_2 capture and storage (CCS). Int. J. Greenhouse Gas Control 31, 1-15. https://doi.org/10.1016/j.ijggc.2014.09.022

Kadu, S.C., Bhushan, M., Gudi, R., 2008. Optimal sensor network design for multirate systems. J Process Control 18, 594-609. https://doi.org/10.1016/j.jprocont.2007.10.002

Kasule, J., Turton R, Bhattacharyya D, Zitney S E, 2014. One-dimensional dynamic modeling of a single-stage downward-firing entrained-flow coal gasifier. Energ. Fuel. 28, 4949-4957. https://doi.org/10.1021/ef5010122

Kasule, J., Turton R, Bhattacharyya D, Zitney S E, 2012. Mathematical modeling of a single-stage, downward-firing, entrained-flow gasifier. Ind. Eng. Chem. Res. Industrial 51, 6429-6440. https://doi.org/10.1021/ie202121h

Kobayashi, T., Simon, D.L., 2003. Application of a bank of Kalman filters for aircraft engine fault diagnostics. ASME Turbo Expo 2003, collocated with the 2003 International Joint Power Generation Conference, 461-470. https://doi.org/10.1115/GT2003-38550

Lee, A.J., Diwekar, U.M., 2012. Optimal sensor placement in integrated gasification combined cycle power systems. Appl. Energ. 99, 255-264. https://doi.org/10.1016/j.apenergy.2012.04.027

Mandela, R.K., Rengaswamy, R., Narasimhan, S., Sridhar, L.N., 2010. Recursive state estimation techniques for nonlinear differential algebraic systems. Chem. Eng. Sci. 65, 4548-4556. https://doi.org/10.1016/j.ces.2010.04.020

Maybeck, P.S., 1982. Stochastic models, estimation, and control. Academic Press, New York.

Mobed, P., Munusamy, S., Bhattacharyya, D., Rengaswamy, R., 2017a. State and parameter estimation in distributed constrained systems. 1. Extended Kalman Filtering of a Special Class of Differential Algebraic Equation Systems. Ind. Eng. Chem. Res. 56, 206-215. https://doi.org/10.1021/acs.iecr.6b02796

Mobed, P., Munusamy, S., Bhattacharyya, D., Rengaswamy, R., 2017b. State and parameter estimation in distributed constrained systems. 2. GA-EKF based sensor placement for a water gas shift reactor. Ind. Eng. Chem. Res. 56, 216-224. https://doi.org/10.1021/acs.iecr.6b02797

Muske, K.R., Georgakis, C., 2003. Optimal measurement system design for chemical processes. AICHE J. 49, 1488-1494. https://doi.org/10.1002/aic.690490612

Musulin, E., Benqlilou, C., Bagajewicz, M.J., Puigjaner, L., 2005. Instrumentation design based on optimal Kalman filtering. J. Process Control 15, 629-638. https://doi.org/10.1016/j.jprocont.2005.03.002

Nabil, M., Narasimhan, S., 2012. Sensor network design for optimal process operation based on data reconciliation. Ind. Eng. Chem. Res. 51, 6789-6797. https://doi.org/10.1021/ie202126q

Nguyen, D., Bagajewicz, M.J., 2012. Efficient approximate methods for the design and upgrade of sensor networks. Ind. Eng. Chem. Res. 52, 83-90. https://doi.org/10.1021/ie202186y

Nguyen, D., Bagajewicz, M.J., 2008. Design of nonlinear sensor networks for process plants. Ind. Eng. Chem. Res. 47, 5529-5542. https://doi.org/10.1021/ie0708778

Paul, P., Bhattacharyya, D., Turton, R., Zitney, S.E., 2017. Nonlinear dynamic model-based multi-objective sensor network design algorithm for a plant with an estimator-based control system. Ind. Eng. Chem. Res. 56, 7478-7490. https://doi.org/10.1021/acs.iecr.6b04020

Paul P., Bhattacharyya D., Turton R., Zitney S. E., 2016. Dynamic model-based sensor network design algorithm for system efficiency maximization. Comput. Chem. Eng. 89, 27-40. https://doi.org/10.1016/j.compchemeng.2016.01.018

Paul P., Bhattacharyya D., Turton R., Zitney S. E., 2015. Sensor network design for maximizing process efficiency: an algorithm and its application. AIChE J. 61, 464-476. https://doi.org/10.1002/aic.14649

Pednekar P, Bhattacharyya D, Turton R, Rengaswamy R, 2016a. Dynamic model of a slagging entrained-flow gasifier including models of slag transport, deposition, and slag layer. Ind. Eng. Chem. Res. 55, 279-292. https://doi.org/10.1021/acs.iecr.5b03317

Pednekar P, Bhattacharyya D, Turton R, Rengaswamy R, 2016b. Development of a hybrid shrinking-core shrinking-particle model for entrained flow gasifiers. AICHE J. 62, 659-669. https://doi.org/10.1002/aic.15055

Ramalakshmi, K., Kaneko, T.K., Mazumdar, B.M., Rozelle, P., Sridhar, S., Kuhlman, J.M., 2014. Infiltration velocity and thickness of flowing slag film on porous refractory of slagging gasifiers. J. Energy Resour. Technol. 136, 032203. https://doi.org/10.1115/1.4026918

Seenumani, G., Dai, D., Lopez-Negrete, R., Kumar, A., Dokucu, M., Kumar, R., 2012. An outer-approximation based algorithm for solving integer non-linear programming problems for optimal sensor placement. 2012 IEEE 51st IEEE Conference on Decision and Control (CDC). Maui. https://doi.org/10.1109/CDC.2012.6426360

Sen, P., Diwekar U. M., Bhattacharyya D. 2018. Stochastic programming approach vs. estimator-based approach for sensor network design for maximizing efficiency. Smart Sustainable Manuf. Syst. 2, 44-60. https://doi.org/10.1520/SSMS20180021

Sen, P., Sen K., Diwekar U. M. 2016. A multi-objective optimization approach to optimal sensor location problem in IGCC power plants. Appl. Energy 181, 527-539. https://doi.org/10.1016/j.apenergy.2016.08.006

Singh, A.K., Hahn, J., 2005. Determining optimal sensor locations for state and parameter estimation for stable nonlinear systems. Ind. Eng. Chem. Res. 44, 5645-5659. https://doi.org/10.1021/ie040212v

Singh, A.K., Hahn, J., 2006. Sensor location for stable nonlinear dynamic systems: multiple sensor case. Ind. Eng. Chem. Res. 45, 3615-3623. https://doi.org/10.1021/ie0511175

Sun, H., Büyüköztürk, O., 2015. Optimal sensor placement in structural health monitoring using discrete optimization. Smart Mater. Struct. 24, 125034. http://doi.org/10.1088/0964-1726/24/12/125034

Washburn, E.W., 1921. The dynamics of capillary flow. Phys. Rev. 17, 273. https://doi.org/10.1103/PhysRev.17.273

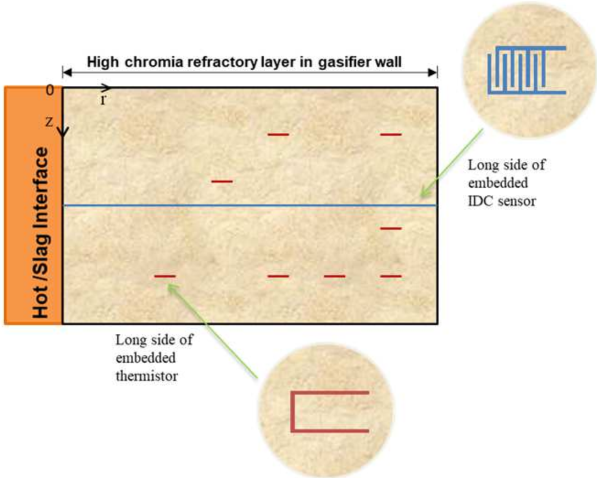

Fig. 12. Graphical abstract